Spatially resolved photoluminescence in quantum wells with interface roughness: a theoretical description

2006 J. Phys.: Condens. Matter 18 2367

(http://iopscience.iop.org/0953-8984/18/8/002)

INSTITUTE OF PHYSICS PUBLISHING JOURNAL OF PHYSICS: CONDENSED MATTER

J. Phys.: Condens. Matter **18** (2006) 2367–2378 doi:10.1088/0953-8984/18/8/002

Spatially resolved photoluminescence in quantum wells with interface roughness: a theoretical description

G Martino[1], **G Pistone, S Savasta, O Di Stefano and R Girlanda**

Istituto Nazionale per la Fisica della Materia INFM and Dipartimento di Fisica della Materia e Tecnologie Fisiche Avanzate, Università di Messina, Salita Sperone 31, I-98166 Messina, Italy

E-mail: giovanna.martino@unime.it

Received 9 September 2005
Published 10 February 2006
Online at stacks.iop.org/JPhysCM/18/2367

Abstract

We present a microscopic theoretical description of spatially resolved photoluminescence in GaAs quantum wells with interface roughness. The theory derives the kinetic equations using the excitonic wavefunctions obtained by solving numerically the effective Schrödinger equation for the excitonic centre of mass motion in the presence of disorder. The kinetic equations describe acoustic phonon scattering, radiative decay, and inhomogeneous sample excitation and/or light detection. The influence of disorder, temperature, and spatial resolution on the image formation is analysed with emphasis on the role of different interface textures. In particular, we consider two samples characterized by effective disorder potentials with different correlation lengths. Numerically calculated two-dimensional images agree with images from spatially resolved photoluminescence experiments and put forward the potential of the method for the understanding of near-field light emission from semiconductor quantum structures.

1. Introduction

Scanning near-field optical microscopy (SNOM) has opened the possibility for studying numerous optical phenomena with resolution well below the diffraction limit [1]. Since in conventional (far-field) optical spectroscopy the light field is essentially constant in amplitude and phase over the spatial extension of the relevant quantum mechanical states, one can measure only an average signal originating from the relatively large surface area determined by the illuminating spot. On the contrary, near-field microscopy and spectroscopy techniques have enormous potential for optical probing of nanostructured materials and are able to probe the morphology and the spatial distribution of optically active quantum states. Among the optical characterization and analysis methods, photoluminescence (PL) is one of the most useful

[1] Author to whom any correspondence should be addressed.

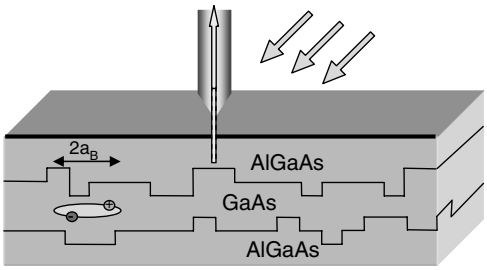

Figure 1. Schematic view of the exciton in a ternary QW with rough interfaces.

and effective means to investigate the optical properties of optically active nanostructured materials. While PL and photoluminescence excitation (PLE) spectroscopy are widely used spectroscopic tools for the optical characterization of semiconductor nanostructures, theoretical simulations generally focus on calculations of local absorption [2–6]. In high quality quantum wells (QWs), electrons relax predominantly by scattering with phonons in a time significantly shorter than the radiative lifetime, thus at low temperature we can see a quite good correspondence between absorption and PLE measurements [7]. However for disordered QWs this correspondence generally breaks down [8]. Disorder in semiconductor heterostructures (due to alloy fluctuations in ternary compounds or geometry) is always present although not always undesired. The nature of QW interfaces can be complex. Entropy and growth kinetic reasons favour irregular shapes and fuzzy boundaries, whereas energetic arguments favour regular compact shapes and straight boundaries [9]. Moreover, the dynamical growth conditions determine regimes of interfacial texture that affect the nature of exciton localization. Layer-by-layer growth determines an interface microroughness with weak short-range potential fluctuations on a length scale much smaller than the exciton radius [10]. By contrast, the Stranski–Krastanov method or growth with interruption of growth [11] produces QD regions where the lateral extent of the confining potential is larger than the exciton diameter. In some cases, disorder with correlation length larger than the Bohr radius is intentionally provoked at the QW interfaces, in order to obtain high quality quantum dots (QDs) [12, 13].

The theory of spatially resolved PL, here presented and applied, includes light quantization, acoustic phonon scattering, and inhomogeneous sample excitation and/or light detection. This framework also allows the description of PL and PLE spectroscopy, in which the excitation and detection energies can all be scanned independently. Moreover, it is possible to model the effects of the illumination and collection spatial resolutions. In particular we calculate spatially resolved PL for two samples, characterized by a different type of interface roughness. Each sample is constituted by a GaAs QW in between $Al_xGa_{1-x}As$ barriers (see figure 1). We present results of absorption, PL and spatially resolved PL in the collection mode configuration for spatial resolutions ranging from 30 to 150 nm. The numerical results here presented clearly evidence the influence of exciton localization due to interface roughness with different length scales in determining the near-field PL images. We also analyse the influence of temperature that plays a relevant role by tuning the competition between radiative and non-radiative scattering.

2. Theory

The optical properties of semiconductor quantum structures are mainly determined by the conduction band and the uppermost valence subbands. To make the situation as simple as

possible we assume a non-degenerate situation, taking into account only a valence and a conduction subband. Furthermore, the subbands are assumed to be isotropic and parabolic with the band minimum localized at the zone centre. The overall effects of the band structure, in particular the fact that the carrier experiences the periodic potential instead of moving in the vacuum, are embodied in the use of an effective mass. Hence the electron energies and wavefunctions can be calculated in the effective mass approximation.

One of the most important problems connected with the growth of heterostructures is structural disorder. In addition to impurities, lattice imperfections, etc, which are also present in these homogeneous bulk crystals, semiconductor quantum structures additionally exhibit interface imperfections which can involve different components with different lateral length scales. Since the disorder in quantum wells determines the breaking of translation symmetry along the free propagation plane of the system, it is convenient to adopt a real-space representation. In reasonably good quality quantum structures the amplitude of the confinement energy fluctuations is typically one order of magnitude smaller than the exciton binding energy [14]. In this limit the electron–hole hydrogen-like relative motion may be assumed to be undistorted by disorder. Disorder significantly affects the centre of mass (COM) motion through an effective potential $V(\mathbf{R})$, where $\mathbf{R}$ indicates the COM vector lying along the well free plane. Owing to these approximations, the exciton wavefunction can be factorized as [14]

$$\Psi_\alpha^{\mathrm{eh}}(z_\mathrm{e}, z_\mathrm{h}, \rho, \mathbf{R}) = u_\mathrm{e}(z_\mathrm{e})u_\mathrm{h}(z_\mathrm{h})\phi_{1\mathrm{s}}(\rho)\psi_\alpha(\mathbf{R}), \tag{1}$$

where $\phi_{1\mathrm{s}}(\rho)$ describes the unperturbed electron–hole (eh) relative motion (ρ being the relative in-plane eh coordinate) corresponding to the lowest exciton transition and $u_{\mathrm{e(h)}}(z_{\mathrm{e(h)}})$ is the confinement function, with $z_{\mathrm{e(h)}}$ being the electron (hole) coordinate along the growth direction. The wavefunctions $\psi_\alpha(\mathbf{R})$ are solutions of the exciton Schrödinger equation written for the COM motion:

$$\left(-\frac{\hbar^2\nabla^2}{2M} + V(\mathbf{R})\right)\psi_\alpha(\mathbf{R}) = \epsilon_\alpha\psi_\alpha(\mathbf{R}), \tag{2}$$

where $M = m_\mathrm{e}^* + m_\mathrm{h}^*$ is the exciton kinetic mass (m_e^* and m_h^* are the effective masses of the electron and the hole).

In a typical luminescence experiment a non-equilibrium distribution of electron–hole (e–h) pairs is initially excited. These optically generated pairs may recombine emitting light or can be scattered inelastically non-radiatively (as a consequence of electron–phonon interaction) to other energy levels. This competition between radiative emission and non-radiative scattering ultimately determines the photoluminescence properties of the system. The microscopic theoretical analysis of this process requires the inclusion of both spontaneous emission and exciton–phonon interaction. Here we also include the description of inhomogeneous sample excitation and/or light detection.

The positive frequency components of the operator describing the signal that can be detected by a general near-field set-up can be expressed as [15, 16]

$$\hat{S}_t^+ = \hat{A}_{\mathrm{bg}}^+ + \hat{S}^+, \tag{3}$$

where $\hat{A}_{\mathrm{bg}}^+$ is the elastic background signal, largely uniform along the xy plane; this term is proportional to the input electric-field operator. $\hat{S}^+$ is related to the sample polarization density operator $\hat{\mathbf{P}}^+(\mathbf{r})$,

$$\hat{S}^+ = \mathcal{A}\int \mathrm{d}\mathbf{r}\,\hat{\mathbf{P}}^+(\mathbf{r})\cdot\mathbf{E}_{\mathrm{out}}(\mathbf{r}), \tag{4}$$

where $\mathcal{A}$ is a complex constant depending on the impedance of the material constituting the tip [15] and $\mathbf{E}_{\rm out}(\mathbf{r})$ is the signal mode delivered by the tip. The interband polarization density operator is given by

$$\hat{\mathbf{P}}^{+}(\mathbf{r}) = \sum_{\rm eh} \boldsymbol{\mu}_{\rm eh}\, \hat{c}_{\rm e}(\mathbf{r})\hat{d}_{\rm h}(\mathbf{r}), \tag{5}$$

where $\boldsymbol{\mu}_{\rm eh}$ is the interband dipole moment and $\hat{c}_{\rm e}(\mathbf{r})$, $\hat{d}_{\rm h}(\mathbf{r})$ are the electron and hole destruction operators in the $\mathbf{r}$-space representation. Photoluminescence can be defined as the incoherent part of the emitted light intensity. The PL that can be measured by a photodetector after the collection set-up (broadband detection) is proportional to $I = \langle \hat{S}^{-}, \hat{S}^{+} \rangle$, (with $\langle \hat{A}, \hat{B} \rangle \equiv \langle \hat{A}\, \hat{B} \rangle - \langle \hat{A} \rangle \langle \hat{B} \rangle$). Analogously the steady-state spectrum of incoherent light emitted by the semiconductor quantum structure and detected by the SNOM set-up can be expressed as

$$I_{\rm PL}(\omega_{\rm out}) = \frac{1}{\pi} \int_{0}^{\infty} {\rm d}\tau\, \langle \hat{S}^{-}(0), \hat{S}^{+}(\tau) \rangle {\rm e}^{{\rm i}\omega_d \tau}. \tag{6}$$

The polarization density operator can be expressed in terms of exciton operators as

$$\hat{\mathbf{P}}^{+}(\mathbf{r}) = \boldsymbol{\mu}_{\rm eh} f(z) \Psi_{\alpha}^{\rm eh}(\rho = 0, \mathbf{R}) \hat{B}_{\alpha} \tag{7}$$

where $f(z) = u_{\rm e}(z) u_{\rm h}(z)$ is the product of the electron and hole envelope functions along the confinement direction (the growth axis) and the operator $\hat{B}_{\alpha}^{\dagger}$ creates an exciton state (one electron–hole pair) $\hat{B}_{\alpha}^{\dagger}|0\rangle \equiv |E_{1,\alpha}\rangle$ with energy $\omega_{1,\alpha}$.

The dynamics controlled truncation scheme [17] provides an upper limit to the number of electron–hole pairs to be included for the dynamics description of the interacting electron system, depending on the excitation density. States with only one electron–hole pair (exciton) are sufficient to describe the system dynamics at low excitation densities. In this regime the following relation can be assumed:

$$\hat{B}_{\alpha} \simeq |0\rangle\langle E_{1,\alpha}|, \tag{8}$$

and it can be shown that the operators $\hat{B}_{\alpha}$ behave as boson operators. Including only the exciton subspace and using equation (8), the Hamiltonian determining the dynamics of the semiconductor system is given by the following three contributions:

$$\hat{\mathcal{H}} = \hat{\mathcal{H}}_0 + \hat{\mathcal{H}}_I + \hat{\mathcal{H}}_s, \tag{9}$$

where the first term is the bare electronic Hamiltonian of the semiconductor system $\hat{\mathcal{H}}_0 = \sum_{\alpha} \hbar\omega_{\alpha} \hat{B}_{\alpha}^{\dagger} \hat{B}_{\alpha}$. The interaction of the semiconductor with the light field (in the usual rotating wave approximation) can be written as

$$\hat{\mathcal{H}}_I = -\int {\rm d}^3 r\, \hat{\mathbf{E}}^{-}(\mathbf{r}) \cdot \hat{\mathbf{P}}^{+}(\mathbf{r}) + {\rm H.c.} \tag{10}$$

We separate the field operator into a classical contribution $\mathbf{E}_{\rm in}(\mathbf{r})$ describing the (possibly inhomogeneous) exciting field and into a fluctuating part $\hat{\mathcal{E}}^{-}(\mathbf{r})$ (the one determining the spontaneous emission) that can be expanded in terms of annihilation photon operators. Finally, $\hat{\mathcal{H}}_s$ describes inelastic scattering due to the interaction of excitons with the phonon bath:

$$\hat{\mathcal{H}}_s = \sum_{\alpha,\beta,\mathbf{q}} t_{\alpha,\beta}^{\mathbf{q}} (\hat{b}_{\mathbf{q}} + \hat{b}_{-\mathbf{q}}^{\dagger}) \hat{B}_{\alpha}^{\dagger} \hat{B}_{\beta}. \tag{11}$$

These terms produce scattering between different exciton states and dephasing. For the lowest exciton states at low temperature, scattering with acoustic phonons is in most cases the dominant process. In particular, at low temperature interaction with optical phonons is efficient at excitations above the bandgap only, because only in this case are total energy and momentum conserved for downward transitions [14, 18]. Therefore, we will include only the

contribution due to acoustic phonons in subsequent numerical calculations. $\hat{b}_{\mathbf{q}}$ is the Bose annihilation operator for a phonon with wavevector $\mathbf{q}$. The scattering matrix elements depend on the lattice deformation potentials and the overlap between the exciton states. The explicit expression for $t^{\mathbf{q}}_{\alpha,\beta}$ can be found elsewhere [19].

The relaxation process in the low-excitation limit can be discussed in terms of kinetic equations for the exciton density matrix. Diagonal terms of the exciton density matrix $N_\alpha = \langle \hat{B}^\dagger_\alpha \hat{B}_\alpha \rangle$ can be derived starting from the Heisenberg equation of motion for the exciton operators

$$-\mathrm{i}\hbar\partial_t \hat{B}^\dagger_\alpha(t) = [\hat{\mathcal{H}}, \hat{B}^\dagger_\alpha(t)] \tag{12}$$

under the influence of $\hat{\mathcal{H}}$.

The main approximations are the neglect of possible coherent phonon states and of memory effects induced by the photon and phonon fields [14]. The resulting kinetic equations that include a spatially inhomogeneous (illumination-mode) input light field of given frequency ω_{in} as input are

$$\partial_t N_\alpha = G_\alpha(\omega_{\mathrm{in}}) + \sum_\beta \gamma_{\alpha\leftarrow\beta} N_\beta - 2\Gamma_\alpha N_\alpha, \tag{13}$$

where $2\Gamma_\alpha = r_\alpha + \sum_\beta \gamma_{\beta\leftarrow\alpha}$ is the total out-scattering rate, r_α is the rate for spontaneous emission proportional to the exciton oscillator strength: $r_\alpha = r_0 |\int \mathrm{d}^2\mathbf{R}\, \psi_\alpha(\mathbf{R})|^2$, and $\gamma_{\beta\leftarrow\alpha}$ are the resulting phonon-assisted scattering rates [14], given by

$$\gamma_{\beta\leftarrow\alpha} = \frac{2\pi}{\hbar} \sum_{\mathbf{q}} \left((n_{\mathbf{q}} + 1)\, \delta\left(\epsilon_\beta + \hbar\omega_{\mathbf{q}} - \epsilon_\alpha\right) + n_{\mathbf{q}} \delta\left(\epsilon_\beta - \hbar\omega_{\mathbf{q}} - \epsilon_\alpha\right) \right) |t^{\mathbf{q}}_{\beta\alpha}|^2. \tag{14}$$

Here we assumed that the tip–sample interaction does not alter the radiative decay rates. In this equation the generation term that describes the specific experimental excitation conditions depends on the spatial overlap between the illuminating beam and the exciton wavefunctions corresponding to exciton levels resonant with the input light [16]:

$$G_\alpha = r_0 \left| o^{\mathrm{in}}_\alpha \right|^2 \mathcal{L}_\alpha(\omega_{\mathrm{in}}) \tag{15}$$

with $\pi \mathcal{L}_\alpha(\omega) = \Gamma/[(\omega - \omega_\alpha)^2 + \Gamma^2]$ and

$$o^{\mathrm{in}}_\alpha = \int \mathrm{d}^2\mathbf{R}\, \tilde{E}_{\mathrm{in}}(\mathbf{R}) \psi_\alpha(\mathbf{R}) \tag{16}$$

where $\tilde{E}_{\mathrm{in}}(\mathbf{R}) = \int E_{\mathrm{in}}(\mathbf{r}) f(z)\, \mathrm{d}z$. This term is proportional to the contribution of an α-exciton level to total absorption under local illumination. In the subsequent numerical calculations, concerning the illumination mode, we will assume an input light field with a given Gaussian profile centred around the tip position: $\tilde{E}_{\mathrm{in}}(\mathbf{R}) = E^0_{\mathrm{in}} g(\mathbf{R} - \bar{\mathbf{R}})$. In this case the generation term becomes a function of the beam position and shape (spatial resolution). We observe that also at steady state equation (13) can give rise to highly non-equilibrium exciton densities. Non-equilibrium here arises from both spontaneous emission that prevents full thermalization and from the eventual local excitation described by the generation terms.

Once the exciton densities have been derived, the frequency integrated PL can be readily obtained.

$$I = r_0 \sum_\alpha \left| o^{\mathrm{out}}_\alpha \right|^2 N_\alpha, \tag{17}$$

where o^{out}_α analogously to o^{in}_α contains the overlap of the exciton wavefunctions with the signal mode $\tilde{E}_{\mathrm{out}}(\mathbf{R})$ delivered by the tip (collection mode) and is given by

$$o^{\mathrm{out}}_\alpha = \int \mathrm{d}^2\mathbf{R}\, \tilde{E}_{\mathrm{out}}(\mathbf{R}) \psi_\alpha(\mathbf{R}). \tag{18}$$

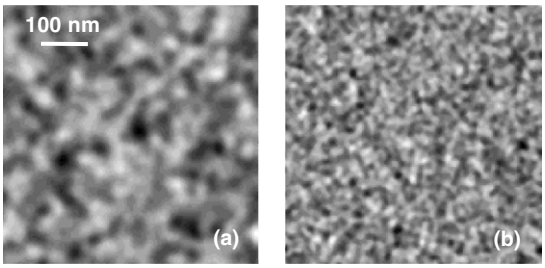

Figure 2. (a) Specific realization of disordered potential obtained summing up two different contributions. (b) Specific realization of disordered potential obtained considering only the contribution with a small correlation length.

According to the quantum regression theorem (see e.g. [20]), $\langle \hat{S}^-(0)\,\hat{S}^+(\tau)\rangle$ has the same dynamics as $\langle \hat{S}^+(\tau)\rangle$ (proportional to the exciton operator), but with $\langle \hat{S}^-(0)\,\hat{S}^+(0)\rangle$ as initial condition. Following this procedure we obtain the spatially and spectrally resolved PL intensity:

$$I_{\mathrm{PL}}(\omega_{\mathrm{out}}) = r_0 \sum_{\alpha} \left|o_{\alpha}^{\mathrm{out}}\right|^2 \mathcal{L}_{\alpha}(\omega_{\mathrm{out}})\, N_{\alpha}. \tag{19}$$

3. Numerical results

We consider a Gaussian stochastic (zero-mean) potential with statistical properties determined by the autocorrelation function [21] $A(\mathbf{R}-\mathbf{R}') = \langle W(\mathbf{R})W(\mathbf{R}')\rangle$, with $A(\mathbf{R}) = v_0^2 \mathrm{e}^{-|\mathbf{R}|^2/2\xi^2}$ where $\langle\cdots\rangle$ denotes an ensemble average over random configurations, v_0 is the amplitude, and ξ is the spatial correlation length characterizing the potential fluctuations. We exploit numerical calculations for two samples characterized by two different kinds of interface roughness, taking into account two different types of disorder occurring in the real structures during the growth process. The samples under consideration are both GaAs single QWs embedded in AlAs barriers. In the first case (sample (a)) we consider at each interface the formation of monolayer islands on the respective surfaces of size larger than the exciton radius (see figure 2(a)). This type of disorder is experimentally achieved by growing QWs with growth interruption on both interfaces. We model this kind of island-like disordered potential $V(\mathbf{R})$ summing up two different stochastic potentials $W(\mathbf{R})$. The first contribution $W_1(\mathbf{R})$ aims to model the monolayer islands and is obtained using values of $\xi = 16$ nm and $v_0 = 2.0$ meV; the second contribution $W_2(\mathbf{R})$ aims to model the background disorder and is obtained using values of $\xi = 7$ nm and $v_0 = 0.2$ meV. The specific realization of the so obtained effective potential (S_a) is shown in figure 2(a). It is worth noting that even in the case of abrupt profiles of fluctuations the resulting effective potential is a smoother function deriving from the convolution of the potential with the 1s exciton wavefunction [22]. The second effective potential (S_b) used for our subsequent calculations models a sample grown without growth interruptions at interfaces. It is obtained by employing only the disorder potential with smaller correlation length $\xi = 7$ nm and an amplitude $v_0 = 2.2$ meV, equal to the sum of the amplitudes used in the previous case for reasons of comparison of the resulting PL spectra. S_b is shown in figure 2(b). However, in both cases the simulation of interface roughness effects on PL and absorption spectra is based on the concept of well-width fluctuations. Indeed, the statistical properties of an interface are usually characterized by two length parameters: the thickness fluctuation and the lateral (in-plane) correlation length [23], as can be observed by direct morphological analysis done, for

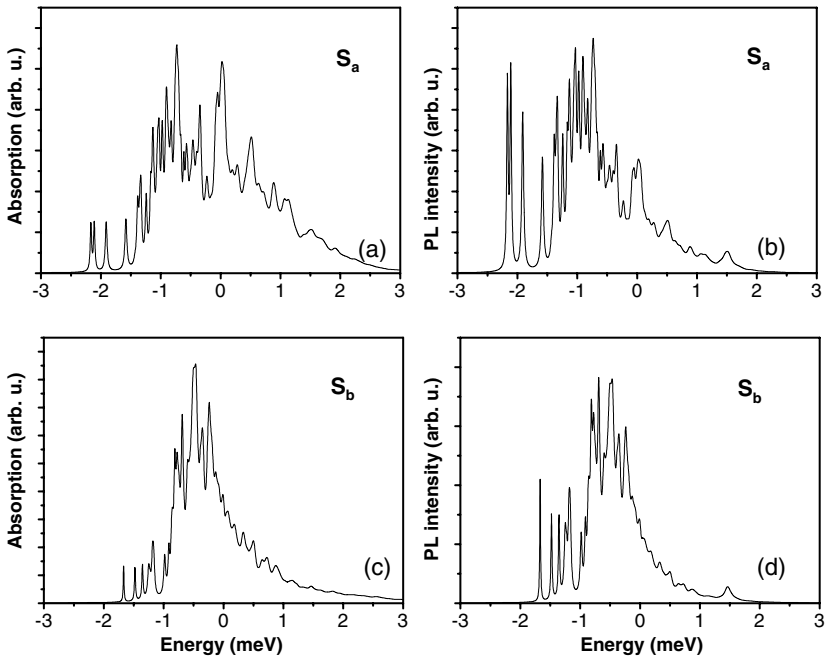

Figure 3. Far-field absorption and photoluminescence spectra for the two samples in figure 2. The temperature of the samples is $T = 10$ K.

instance, with cross-sectional scanning tunnel microscopy [24], scattering ellipsometry [25], and x-ray reflection measurements [26, 27].

Calculations are carried out in real space mapping on a fine mesh of points the Hamiltonian $\hat{\mathcal{H}}$ (see equation (9)), which is then diagonalized in order to obtain eigenvalues and eigenvectors. An exciton kinetic mass of $m = 0.25\ m_0$, typical for AlAs/GaAs QWs, has been used. The spectra have been calculated by considering a square region of 540 nm by 540 nm which has been reproduced by a 90×90 mesh. Periodic boundary conditions have been adopted.

SNOM PL spectra are very sensitive to the mode of operation [16]. In the experimental set-up that we model, calculations are performed in the collection mode configuration, where the samples are illuminated in far field and the resulting luminescence is collected locally using the fibre probe. Figure 1 shows a schematic view of the exciton in the ternary AlAs/GaAs QW for S_a and the experimental set-up for the collection mode configuration. Before showing PL images, in figure 3 we report for reference far-field absorption and PL spectra calculated at the temperature of 10 K for the two samples. The obtained far-field spectra are far from being a smooth band. This originates from the reduced number of emitting centres owing to the smallness of the sample employed for simulations (540×540 nm^2). For both samples two distinct regions related to the effective mobility edge for exciton relaxation [28] can be observed. At lower energy we can distinguish generally sharper distinct peaks, while at higher energy peaks are generally larger due to a more effective phonon-induced scattering. We also observe a noticeable difference between PL and absorption spectra for both samples, originating from the fact that for states at high energy, relaxation due to phonon scattering is much more rapid then the radiative decay rate [29]. Figure 4 displays energy-integrated PL images obtained after uniform illumination of the sample at energy $\omega_I = 1$ meV (the zero of energy is fixed at the energy of the 1s exciton in the absence of disorder) and locally collecting the emitted light with spatial resolution FWHM $= 30$ nm at different temperatures.

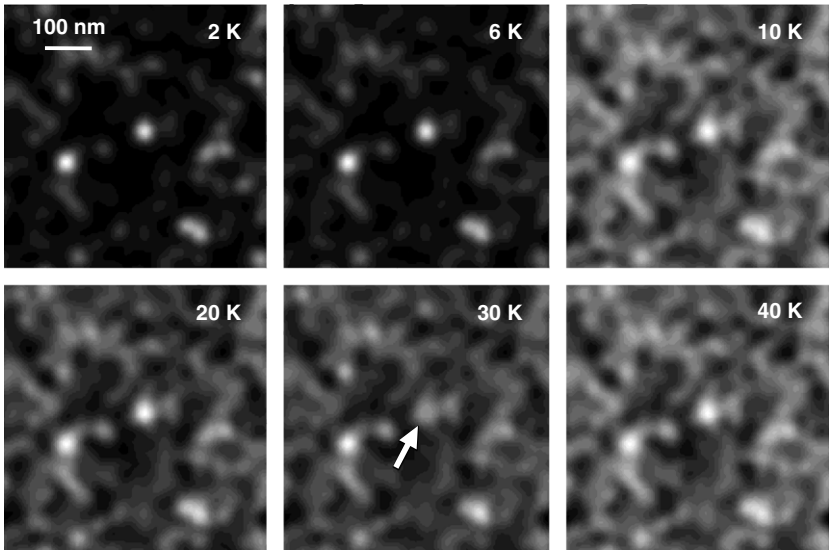

Figure 4. Energy-integrated PL images obtained after uniform illumination of the sample shown in figure 2(a) at energy $\omega_I = 1$ meV and collecting locally the emitted light with a spatial resolution of 30 nm at six different temperatures.

It is worth noting that the energy integrated excitonic local density of states does not depend on position. So the observed emitting structures are a direct consequence of the increasing ratio between radiative and non-radiative scattering rates for exciton states localized at the potential minima (compare e.g. images of figure 2(a) with figure 4). As the temperature of the structure is lowered, a transition from a broad and fairly continuous PL to an intense set of a few spatially localized luminescence centres can be observed. In particular, at low temperature emission originates mainly from the potential minima and gives information on the potential profile of the sample (see figures 2(a) and 4). Such a localization of light emission has been observed in measurements of low-temperature spatially resolved PL [30–32]. Another interesting feature is the non-monotonic brightness of some luminescence centres when the temperature is increased (see e.g. the location indicated by an arrow in the image at 30 K in figure 4). When temperature increases, excitons can overcome shallow local minima by thermal activation and fall into still deeper states. This mechanism is also at the basis of the interpretation of the observed non-monotonic Stokes shift of PL spectra in dependence on temperature [33–37]. The spatially resolved effect here observed can be regarded as the microscopic evidence of this mechanism and supports this interpretation.

Figure 5 displays energy integrated spatially resolved photoluminescence obtained for two different temperatures of S_a ($T = 4$ and 40 K) and collecting the emitted light at different spatial resolutions. The images calculated using a full width at half maximum (FWHM) of 30 nm give information on the spatial extension of the quantum states of spatially localized luminescence centres and partially determine their inner structure. In order to investigate the impact that spatial resolution may have on the local spectra, we present the photoluminescence spectrum of S_a for three different values of FWHM. This behaviour is not merely an average effect but it also originates from spatial interference of the corresponding quantum states due to the nonlocal character of light–matter interaction in semiconductors.

It can be instructive to better understand the importance of the specific realization of the potential to the luminescence images to compare early results with those obtained for S_b,

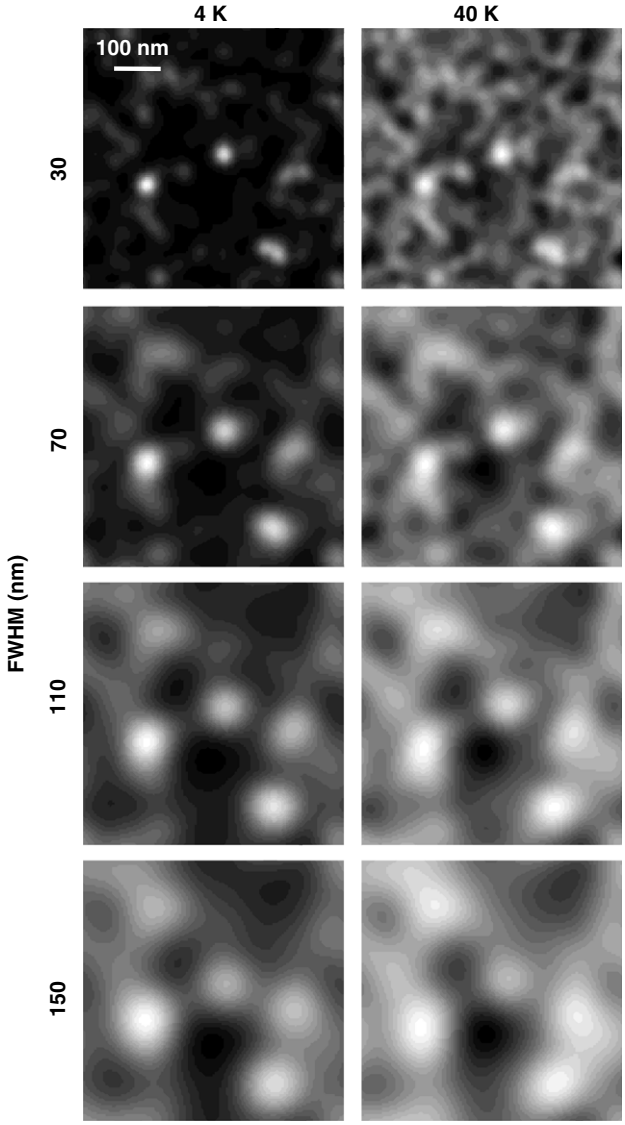

Figure 5. Energy integrated spatially resolved photoluminescence when sample (a) in figure 2 has a temperature of $T = 4$ and 40 K for different spatial resolutions.

characterized by white-noise-like disorder with potential fluctuations at scale length of the order of magnitude of the exciton Bohr radius. In this case the spatial resolution used for the simulation is too low in order to obtain information about the potential. We also observe that such a type of disorder is not able to confine the excitons in the single minima of the potential so we expect to obtain information on the spatial extension of the excitonic quantum states and partially determine their inner structure. Figure 6 shows energy-integrated images obtained for S_b in collection mode configuration. As the temperature of the structure is lowered, a transition from a broad and fairly continuous PL to less continuous luminescence centres can be observed but, as expected, at low temperature emission does not originate exclusively from the potential

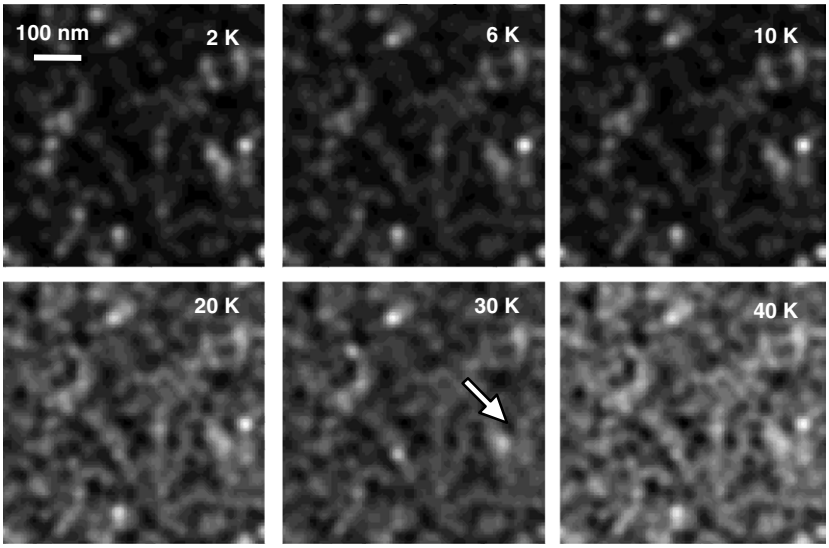

Figure 6. Energy-integrated PL images obtained after uniform illumination of the sample shown in figure 2(b) at energy $\omega_I = 1$ meV and collecting locally the emitted light with a spatial resolution of 30 nm at six different temperatures.

minima as happened in sample S_a. The greater randomness of the disorder in the structure gives rise to a loss of information on the potential profile (compare images of figures 2(b) and 5). This is mainly due to the fact that the greater spatial resolution adopted (FWHM 30 nm) is larger than the potential fluctuations. This leads to an averaging process in optical response, as can be seen by comparing figures 4 and 6 with two images of potentials S_a and S_b. Moreover, the rapid fluctuations of the potential give rise to an Anderson-like localization of excitons of different nature from localization due to quantum confinement of excitons in the potential minima observed in S_a. We also observe that, in analogy to what happens for S_a, increasing temperature, excitons are thermally activated and fall down in still deeper states. Also for S_b we observe a non-monotonic brightness of some luminescence centres when the temperature is increased (see e.g. the location indicated by an arrow in the image at 30 K in figure 6).

Figure 7 displays energy integrated spatially resolved photoluminescence obtained for two different temperatures of S_b ($T = 4$ and 40 K) and collecting the emitted light at different spatial resolutions. We note that the behaviour is qualitatively similar to that of S_a giving, at a FWHM of 30 nm resolution, information on the spatial extension of the quantum states of spatially localized luminescence centres, but at high values of FWHM we can observe a more negligible effect of the temperature on PL spectra.

We conclude that for S_a the enhancement of spatial resolution up to 30 nm is crucial to map both the real-space distribution of eigenstates within QDs and the potential profile; instead for S_b it is not possible to obtain information about the potential but it is still possible to map the excitonic eigenfunctions.

4. Conclusion

In this paper we have presented numerical calculations of spatially resolved photoluminescence in QWs with interface roughness under steady-state conditions. We have modelled two GaAs single QWs embedded in AlAs barriers obtained with or without growth interruption. We

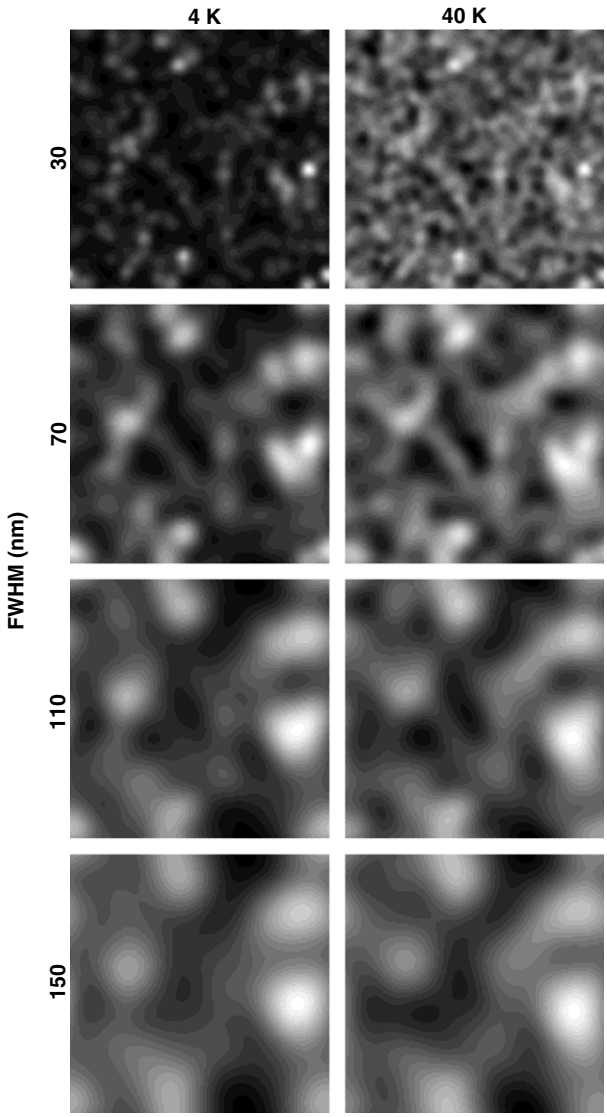

Figure 7. Energy integrated spatially resolved photoluminescence when sample (b) in figure 2 has a temperature of $T = 4$ and 40 K for different spatial resolutions.

have focused on exciton localization related to interface roughness. Moreover, we have studied the effect of temperature and of spatial resolution on the exciton photoluminescence images obtained after uniform illumination of the sample and local collection of the emitted light. The direct comparison of local spectra obtained with two realized disorder potentials yields characteristic signatures and puts forward the correlation between structural disorder, sample temperature and spatial resolution on near-field PL images. Also, our computational tool is suitable for importing any kind of numerically modelled disordered potential, so giving the opportunity to perform future calculations using more and more realistic models. Finally, it is worthy of note that the theory here presented can be applied to study photosensitive quantum systems, of great topicality.

References

[1] Courjon D 2003 *Near-Field Microscopy and Near-Field Optics* (London: Imperial College Press)
[2] Mauritz O, Goldoni G, Rossi F and Molinari E 1999 *Phys. Rev. Lett.* **82** 847
[3] Di Stefano O, Savasta S, Martino G and Girlanda R 2000 *Appl. Phys. Lett.* **77** 2804
[4] Savasta S, Martino G and Girlanda R 2000 *Phys. Rev.* B **61** 13852
[5] Di Stefano O, Savasta S, Martino G and Girlanda R 2000 *Phys. Rev.* B **62** 11071
[6] Hohenester U, Goldoni G and Molinari E 2004 *Appl. Phys. Lett.* **84** 3963
[7] Yu P Y and Cardona M 1999 *Fundamentals of Semiconductors* (Berlin: Springer)
[8] Zimmermann R, Große F and Runge E 1997 *Pure Appl. Chem.* **69** 1179
[9] Jahn U, Kwok S H, Ramsteiner M, Hey R and Grahn H T 1996 *Phys. Rev.* B **54** 2733
[10] Flack F, Samarth N, Nikitin V, Crowell P A, Levy J S and Awschalom D D 1996 *Phys. Rev.* B **54** R17312
[11] Langbein W, Leosson K, Jensen J R, Hvam J M and Zimmermann R 2000 *Phys. Rev.* B **61** R10555
[12] Gammon D, Snow E S and Katzer D S 1995 *Appl. Phys. Lett.* **67** 2391
[13] Gammon D, Snow E S, Shanabrook B V, Katzer D S and Park D 1996 *Phys. Rev. Lett.* **76** 3005
Gammon D, Snow E S, Shanabrook B V, Katzer D S and Park D 1996 *Science* **273** 87
[14] Zimmermann R, Runge E and Savona S 2003 Theory of resonant secondary emission: Rayleigh scattering versus luminescence *Quantum Coherence, Correlation and Decoherence in Semiconductor Nanostructures* ed T Takagahara (USA: Elsevier Science) pp 89–165
[15] Greffet J-J and Carminati R 1997 *Prog. Surf. Sci.* **56** 133
[16] Pistone G, Savasta S, Di Stefano O and Girlanda R 2004 *Appl. Phys. Lett.* **84** 2971
[17] Axt V M, Victor K and Stahl A 1996 *Phys. Rev.* B **53** 7244
[18] Siantidis K, Axt V M and Kuhn T 2001 *Phys. Rev.* B **65** 035303
[19] Runge E and Zimmermann R 1998 *Phys. Status Solidi* b **206** 167
[20] Mandel L and Wolf E 1995 *Optical Coherence and Quantum Optics* (Cambridge: Cambridge University Press)
[21] Glutsch S, Chemla D S and Bechstedt F 1996 *Phys. Rev.* B **54** 11592
[22] Castella H and Wilkins J W 1998 *Phys. Rev.* B **58** 16186
[23] Ponomarev I V, Deych L I and Lisyansky A A 2005 *Phys. Rev.* B **71** 155303
[24] Yayon Y, Esser A, Rappaport M, Umansky V, Shtrikman H and Bar-Joseph I 2002 *Phys. Rev. Lett.* **89** 157402
[25] Germer T A 2000 *Phys. Rev. Lett.* **85** 349
[26] Holý V and Baumbach T 1994 *Phys. Rev.* B **49** 10668
[27] Kondrashkina E A, Stepanov S A, Opitz R, Schmidbauer M, Kohler R, Hey R, Wassermeier M and Novikov D V 1997 *Phys. Rev.* B **56** 10469
[28] Jahn U, Ramsteiner M, Hey R, Grahn H T, Runge E and Zimmermann R 1997 *Phys. Rev.* B **56** R4387
[29] Kocherscheidt G, Langbein W, Woggon U, Savona V, Zimmermann R, Reuter D and Wieck A D 2003 *Phys. Rev.* B **68** 085207
[30] Wu Q, Grober R D, Gammon D and Katzer D S 2000 *Phys. Status Solidi* b **221** 505
[31] Wu Q, Grober R D, Gammon D and Katzer D S 1999 *Phys. Rev. Lett.* **83** 2652
[32] Hess H F, Betzig E, Harris T D, Pfeiffer L N and West K W 1994 *Science* **264** 1740
[33] Skolnick M S, Tapster P R, Bass S J, Pitt A D, Apsley N and Aldred S P 1986 *Semicond. Sci. Technol.* **1** 29
[34] Davey S T, Scott E G, Wakefield B and Davies G J 1988 *Semicond. Sci. Technol.* **3** 365
[35] Daly E M, Glynn T J, Lambkin J D, Considine L and Walsh S 1995 *Phys. Rev.* B **52** 4696
[36] Zimmermann R and Runge E 1997 *Phys. Status Solidi* a **164** 511
[37] Zimmermann R, Runge E and Grosse F 1996 *Proc. 23rd Int. Conf. on the Physics of Semiconductors (Berlin, 1996)* vol 3, ed M Scheffler and R Zimmermann (Singapore: World Scientific) p 1935